ELSEVIER

Journal of Archaeological Science 31 (2004) 1349–1359

Journal of Archaeological SCIENCE

http://www.elsevier.com/locate/jas

Small-angle X-ray scattering: a high-throughput technique for investigating archaeological bone preservation

J.C. Hiller[a,*], M.J. Collins[b,1], A.T. Chamberlain[c,2], T.J. Wess[a]

[a] *Biophysics Group, Department of Optometry and Vision Sciences, University of Cardiff, Cardiff CF10 3NB, UK*
[b] *BioArch, Departments of Archaeology and Biology, University of York, York YO1 7EP, UK*
[c] *Department of Archaeology, University of Sheffield, Sheffield S1 4ET, UK*

Received 9 May 2003; received in revised form 27 January 2004

Abstract

Diagenetic alteration to archaeological bone can cause significant disruption to both the biogenic mineral structure and the preservation of biomolecular resources such as protein and DNA over archaeological time. We report here the use of a technique, small-angle X-ray scattering, which makes it possible to examine the alteration to the mineral surface due to diagenesis. This method has previously been applied to archaeological bone thin sections, but has been modified in this case for use on bone powder as a high-throughput screening technique for bone preservation. Our results show that mineral structural change is not necessarily reflected in the currently used methods of measuring lattice perfection, and that the preservation of archaeological biomolecules may be linked to structural alteration as much as to crystallinity.

Keywords: Diagenesis; Bone preservation; SAXS; Biomolecular archaeology

1. Introduction

Bone is an important resource in the archaeological record that is increasingly subject to a variety of chemical and biomolecular analyses to extract additional information regarding the past. Bone is a composite material, consisting of a mineral phase (primarily carbonated hydroxyapatite) embedded in and overgrowing an organic fraction composed primarily of collagen. Archaeological collagen has been extracted for use in radiocarbon dating and stable isotope studies involving both animal and human remains (e.g. [1]; and others). Kinship, individual characteristics, and evolutionary relationships have been studied in the archaeological record using DNA (e.g. [10]; and others). More recently, the use of osteocalcin sequences to establish evolutionary relationships promises to extend molecular phylogenetics into geological time [28]. Further, the mineral component of bone has been suggested as an alternative material for relative [22,32] and absolute [25] dating.

Diagenetic change over archaeological time profoundly affects the usefulness of bone samples as sources of informative biomolecular material. The influence of diagenetic processes on organic material in bone has been the subject of much research (e.g. [7,18]). In addition, the verification of results by confirmation of a high level of organic preservation in the bone has become an important hallmark of biomolecular archaeological research [9]. Screening techniques for assessing the state of bone preservation before pressing forward with the complex and error-prone processes of biomolecular retrieval have been adopted to save time and expense [24,30].

It has been posited that binding to bone mineral stabilizes some biomolecules such as osteocalcin; this contributes to their persistence in the archaeological record [5,6,17]. Additionally, the association of collagen with bone mineral renders the protein biologically

* Corresponding author. Tel.: +44-29-2087-0204; fax: +44-29-2087-4859.

E-mail addresses: hillerj@cardiff.ac.uk (J.C. Hiller), mc80@york.ac.uk (M.J. Collins), a.chamberlain@sheffield.ac.uk (A.T. Chamberlain), westj@cardiff.ac.uk (T.J. Wess).

[1] Tel.: +44-1904-433901; fax: +44-1904-433902.

[2] Tel.: +44-114-222-2906; fax: +44-114-272-2563.

0305-4403/$ - see front matter © 2004 Published by Elsevier Ltd.
doi:10.1016/j.jas.2004.02.013

unavailable for microbial degradation [4,7]. Biological demineralisation and deterioration, interaction with groundwater, and chemical degradation of the protein chains all contribute to the loss of collagen in archaeological bone [8,19,21].

Due to the importance of bone mineral in the preservation of biomolecular information over archaeological time, screening techniques that examine the diagenetic state of the mineral fraction have been developed. These include the use of Fourier-transform infrared spectra (FTIR) to calculate indices of crystal change (e.g. [40,41]); X-ray diffraction (XRD) to determine crystal composition and strain and bone density (e.g. [12,29]); and particle-induced X-ray emission (PIXE) to examine diagenetic chemical substitutions in the mineral structure [31], among others. A correlation between the FTIR splitting factor (defined in [35]) and the level of organic preservation represented by weight percent nitrogen has been shown [33], reinforcing the view that alteration to the mineral component of bone contributes to the loss of the organic component. Moreover, it has been suggested that DNA preservation in archaeological remains could also be subject to change in the mineral component [16]. There is evidence to suggest, however, that the results of some of the techniques employed to measure mineral alteration can be partially dependent on sample preparation procedures [34].

The use of a technique developed to examine crystallite nanostructure in a range of materials has recently found a new application in the study of mineral change in archaeological bone. This method, small-angle X-ray scattering (SAXS), allows for the accurate determination of crystal size, shape, and orientation within bone independent of crystal lattice perfection [14,15,37]. SAXS has been shown to provide information regarding crystallite structure that is complementary to other techniques employed in archaeological contexts [3] and recently has been used to characterize diagenetic change in bone and other materials of archaeological interest [38,39]. The measurement of subtle changes to crystallite thickness or shape could provide a window to the events leading to mineral alteration in archaeological bone, including diagenetic processes as well as human interventions such as burning. Additionally, it might provide a means to determine whether a threshold exists, beyond which further crystal alteration jeopardizes the protection of organic material in the bone matrix over archaeological time.

We have recently acquired an in-house X-ray scattering apparatus, capable of both SAXS measurements and wide-angle X-ray scattering (WAXS) measurements, which mimic traditional XRD. This facility is devoted to the study of both wet and dry collagenous material, including tendon, historical parchment, and modern and archaeological bone. Its straightforward sample preparation and relatively quick data collection process have allowed us to develop a high-throughput SAXS procedure for the study of mineral alteration in bone. In this study, we present the results of our initial work on a series of modern and archaeological samples from a variety of sources, along with corresponding measurements of diagenetic alteration such as FTIR splitting factor (SF), weight percent nitrogen, and carbonate: phosphate ratio in bone mineral. We aim to show that the development of SAXS as a swift, simple, and statistically robust technique to measure crystal change in archaeological bone contributes substantially to our understanding of processes of mineral alteration and the preservation of organic material in bone over time.

2. Methods and materials

Three modern samples were used as controls. One was a bone from a modern bear, obtained from the osteological reference collections of the Hancock Museum, Newcastle upon Tyne, UK. A small rectangular fragment of cortical bone was sampled from the mandible of the bear, and the remainder of the specimen was returned to the collections. The other two reference samples are modern human cortical bone samples made available from the teaching collections of the Department of Archaeology and Prehistory, University of Sheffield, UK. The modern bone samples were defatted in a 1:1 chloroform:methanol mixture using sonication, and allowed to dry overnight in a fume hood. Processing of modern bone into powder was done in a fume hood.

A series of archaeological bone samples collected as part of a larger study into the preservation of bone material in cave sites was used in this research. Details of the samples, including species, provenance, and approximate date, are provided in Table 1. All bones were processed into finely ground powders by hand using an agate mortar and pestle.

For SAXS measurements, powdered samples (approximately 15 mg) were loaded into a sample carriage between two mica sheets and mounted in the vacuum chamber of the NanoSTAR (Bruker AXS, Karlsruhe) X-ray facility at Cardiff University. The data collection procedure used followed that described in detail in [38]. Scattering profiles were taken over 3 h exposures using a sample to detector distance of 1.25 m. Collected data were corrected for camera distortions, a background image was subtracted, and images were analysed using in-house software. The two-dimensional detector output was converted into spherically averaged one-dimensional profiles. Values for crystal thickness (T) of the smallest dimension, as well as curves describing crystallite morphology and a shape parameter (η), were determined for each sample using the SAXS data. A detailed procedure for these calculations is presented in [13,14]. For a crystallite of dimensions a, b, and c, where c is much larger than a and b, the thickness

Table 1
Details of samples used, including species, provenance, age, and diagenetic data (the final column indicates the results of the sample in ancient DNA experiments: Y is a positive yield, N is no result, and U is untested)

Sample	Site	Species	Date (bp)	Thickness (nm)	SF	C:P	% Nitrogen	DNA (Y/N/U)
mHSS1	n/a	*Homo sapiens*	Modern	3.82	2.72	0.445	4.17	U
mHSS2	n/a	*Homo sapiens*	Modern	4.58	2.86	0.363	4.36	U
TWM1	n/a	Ursid (unidentified)	Modern	2.97	2.82	0.338	4.1	U
SC5E-362	Scladina Cave interior	*Ursus spelaeus*	90–130,000	3.63	3.35	0.255	0.19	U
SC5E-34a	Scladina Cave interior	*Ursus spelaeus*	90–130,000	3.94	3.17	0.252	0.155	U
SC5E-34b	Scladina Cave interior	*Ursus spelaeus*	90–130,000	4.17	3.1	0.267	0.185	U
SC5E-36a	Scladina Cave interior	*Ursus spelaeus*	90–130,000	4.42	3.3	0.236	0.305	U
SC5E-36b	Scladina Cave interior	*Ursus spelaeus*	90–130,000	2.93	3.04	0.273	0.495	U
SC5F-30	Scladina Cave interior	*Ursus spelaeus*	90–130,000	3.88	3.13	0.263	0.2	U
SCVb81-90a	Scladina Cave terrace	*Ursus spelaeus*	90–130,000	3.38	3.1	0.426	0.12	U
SCVb81-90b	Scladina Cave terrace	*Ursus spelaeus*	90–130,000	3.95	3.28	0.799	0.245	U
SCVb81-91	Scladina Cave terrace	*Ursus spelaeus*	90–130,000	3.98	3.6	0.611	0.735	U
SCVb81-130	Scladina Cave terrace	*Ursus spelaeus*	90–130,000	4.34	3.28	0.535	0.67	U
SCVb82-346	Scladina Cave terrace	*Ursus spelaeus*	90–130,000	5.79	2.9	0.372	0.405	U
SCVb81-78	Scladina Cave terrace	*Ursus spelaeus*	90–130,000	2.77	2.94	0.387	0.4	U
SC95F38	Scladina Cave interior	*Ursus spelaeus*	10–40,000	2.96	2.85	0.414	2.52	U
SC91C39	Scladina Cave interior	*Ursus spelaeus*	10–40,000	3.44	2.93	0.37	2.185	U
SC2KG32	Scladina Cave interior	*Ursus spelaeus*	40–75,000	3.50	3.04	0.327	1.14	U
SC99D41	Scladina Cave interior	*Ursus spelaeus*	40–75,000	3.78	3.1	0.302	0.72	U
SC99E36	Scladina Cave interior	*Ursus spelaeus*	40–75,000	4.41	2.94	0.333	0.71	U
SC94W28	Scladina Cave interior	*Ursus spelaeus*	40–75,000	3.30	3.11	0.335	0.855	U
SC99B38	Scladina Cave interior	*Ursus spelaeus*	80–100,000	5.76	3.1	0.325	1.135	U
SC99E34	Scladina Cave interior	*Ursus spelaeus*	80–100,000	4.61	3.49	0.219	1.84	U
SC99F9	Scladina Cave interior	*Ursus spelaeus*	90–130,000	4.56	2.98	0.548	0.39	U
SC90G23	Scladina Cave interior	*Ursus spelaeus*	>130,000	8.16	2.98	0.353	0.755	U
SC2K247	Scladina Cave interior	*Ursus spelaeus*	>130,000	5.09	3.24	0.26	0.79	U
SC2K221	Scladina Cave interior	*Ursus spelaeus*	>130,000	4.52	2.84	0.3	0.915	U
SC11700	Scladina Cave interior	*Ursus spelaeus*	80–100,000	3.59	2.86	0.378	2.31	Y
SC14200	Scladina Cave interior	*Ursus arctos*	80–100,000	3.69	2.8	0.427	3.41	N
SC95456	Scladina Cave interior	*Ursus spelaeus*	Unknown	3.74	3.02	0.299	2.26	N
SC92152	Scladina Cave interior	*Ursus spelaeus*	Unknown	3.96	2.98	0.327	2.3	N
SP-005	La Balme à Collomb	*Ursus spelaeus*	Unknown	3.23	3	0.333	2.84	N
SP-006	La Balme à Collomb	*Ursus spelaeus*	Unknown	3.57	3.04	0.29	0.25	N
SP-007	La Balme à Collomb	*Ursus spelaeus*	Unknown	4.86	3.3	0.276	0.35	N
CPC2320	Carsington Pasture Cave	*Equus equus*	>3900	3.61	2.9	0.34	1.595	U
CPC2311	Carsington Pasture Cave	*Bos taurus*	>3900	3.05	2.9	0.41	1.51	U
CPC2335	Carsington Pasture Cave	*Capra hircus*	>3900	3.56	3.2	0.338	1.44	U
CPC2310	Carsington Pasture Cave	*Bos taurus*	>3900	3.76	3.4	0.245	1.305	U
CPC321	Carsington Pasture Cave	*Homo sapiens*	>3900	2.78	2.8	0.547	3.92	U
CPC324	Carsington Pasture Cave	*Homo sapiens*	>3900	3.87	3.2	0.358	1.425	U
CPC2337	Carsington Pasture Cave	*Capreolus* sp.	>3900	2.45	2.7	0.733	3.075	U
AX 594	Amtuxate Cave	*Ursus spelaeus*	30,000	4.39	3.5	0.316	0.175	U
AX 613	Amtuxate Cave	*Ursus spelaeus*	30,000	4.35	3.2	0.268	0.255	U
AX 596	Amtuxate Cave	*Ursus spelaeus*	30,000	4.24	3.3	0.255	0.15	U
AX 843	Amtuxate Cave	*Ursus spelaeus*	30,000	3.70	3.1	0.306	0.99	U
LU-S 367	La Lucia hall site	*Ursus spelaeus*	76–85,000	4.54	3.6	0.215	0.13	U
LU-S 309	La Lucia hall site	*Ursus spelaeus*	76–85,000	5.47	3.86	0.145	0.1	U
LU-S 403	La Lucia hall site	*Ursus spelaeus*	76–85,000	3.91	3.4	0.236	0.125	U
LU-S 447	La Lucia hall site	*Ursus spelaeus*	76–85,000	4.17	3.8	0.115	0.215	U
LU-S 421	La Lucia hall site	*Ursus spelaeus*	76–85,000	3.72	3.3	0.273	1.2	U
LU-R 766	La Lucia ramp site	*Ursus deningeri*	320,000	3.83	3.16	0.275	0.115	U
LU-R 1078	La Lucia ramp site	*Ursus deningeri*	320,000	5.11	3.5	0.225	0.13	U
LU-R 769	La Lucia ramp site	*Ursus deningeri*	320,000	4.69	3.2	0.286	0.12	U
LU-R 1113	La Lucia ramp site	*Ursus deningeri*	320,000	4.35	3.3	0.201	0.09	U
LU-R 910	La Lucia ramp site	*Ursus deningeri*	320,000	4.79	3.3	0.233	0.14	U
T 7215	El Reguerillo Cave	*Ursus spelaeus*	160,000	4.17	3.19	0.238	0.195	U
T 7216	El Reguerillo Cave	*Ursus spelaeus*	160,000	3.85	3.1	0.256	0.35	U
T 6235	El Reguerillo Cave	*Ursus spelaeus*	160,000	5.08	3.4	0.191	0.18	U
T 7110	El Reguerillo Cave	*Ursus spelaeus*	160,000	4.17	3.3	0.226	0.16	U
T 6766	El Reguerillo Cave	*Ursus spelaeus*	160,000	4.17	2.9	0.287	0.125	U

(*continued on next page*)

Table 1 (*continued*)

Sample	Site	Species	Date (bp)	Thickness (nm)	SF	C:P	% Nitrogen	DNA (Y/N/U)
WIER6871	Wierchowska Gorna	*Panthera spelaea*	Unknown	5.29	3.07	0.344	1.445	U
WIER6867	Wierchowska Gorna	*Panthera spelaea*	Unknown	147.11	3.13	0.366	2.925	U
WIER5710	Wierchowska Gorna	*Panthera spelaea*	Unknown	6.52	2.9	0.324	2.48	U
WIER6804	Wierchowska Gorna	*Panthera spelaea*	Unknown	6.80	3.2	0.252	2.22	U
WIER6792	Wierchowska Gorna	*Panthera spelaea*	Unknown	5.62	3.16	0.289	0.51	U
WIER6807	Wierchowska Gorna	*Panthera spelaea*	Unknown	7.20	3.07	0.259	0.075	U
WIER6805	Wierchowska Gorna	*Panthera spelaea*	Unknown	6.69	3.06	0.27	1.495	U
WIER6878	Wierchowska Gorna	*Panthera spelaea*	Unknown	4.60	2.96	0.414	3.675	U
WIER6798	Wierchowska Gorna	*Panthera spelaea*	Unknown	8.58	3.1	0.314	0.58	U
RAJ 167	Jaskinia Raj	*Coelodonta antiquitatis*	40–60,000	5.33	3.1	0.588	0.685	U
RAJ 1371	Jaskinia Raj	*Ursus spelaeus*	40–60,000	9.07	3.6	0.37	0.595	U
RAJ STZOL	Jaskinia Raj	*Crocuta spelaea*	40–60,000	6.72	3.04	0.39	3.475	U
BP-1	Charterhouse Warren Farm	*Bos primigenius*	3605±45	4.31	3.05	0.327	1.31	Y
BP-2	Totty Pot	*Bos primigenius*	6540±45	4.42	3.35	0.255	0.91	Y
BP-3	Carsington Pasture Cave	*Bos primigenius*	5145±70	2.48	2.7	0.462	3.84	Y
RC 1	Reindeer Cavern	*Rangifer tarandus*	90,000	4.54	3.2	0.362	1.395	U
RC 2	Reindeer Cavern	*Rangifer tarandus*	90,000	3.55	2.98	0.396	2.09	U
MH A	Totes Gebirge 1, Austria	*Ursus spelaeus*	45,000	2.72	2.85	0.396	3.015	Y
MH B	Totes Gebirge 2, Austria	*Ursus spelaeus*	50,000	2.46	2.78	0.433	3.07	Y
MH C	Totes Gebirge 1, Austria	*Ursus spelaeus*	32,000	2.39	2.78	0.411	3.325	Y
MH D	Vindija, Croatia	*Ursus spelaeus*	80–90,000	3.70	3.23	0.241	0.265	N
MH E	Vindija, Croatia	*Ursus spelaeus*	40–50,000	2.99	3.04	0.299	0.56	N
MH F	Vindija, Croatia	*Ursus spelaeus*	35,000	4.14	3.36	0.263	0.335	N
MH G	Vindija, Croatia	*Ursus spelaeus*	35,000	4.16	3.12	0.242	1.905	N
MH I	Totes Gebirge 1, Austria	*Ursus spelaeus*	45,000	2.84	2.75	0.437	3.425	Y
MH J	Vindija, Croatia	*Ursus spelaeus*	40–50,000	2.89	3.16	0.276	0.25	N
MH K	Vindija, Croatia	*Ursus spelaeus*	40–50,000	3.27	3.16	0.265	0.155	N
MH M	Totes Gebirge 2, Austria	*Ursus spelaeus*	44,000	3.47	2.96	0.323	2.365	N
MH N	Totes Gebirge 1, Austria	*Ursus spelaeus*	37,000	4.69	2.96	0.31	1.94	N
MH P	Vindija, Croatia	*Ursus spelaeus*	40–50,000	3.80	3.2	0.222	0.235	N
MH Q	Totes Gebirge 2, Austria	*Ursus spelaeus*	50,000	2.67	2.78	0.761	3.165	Y
MH R	Totes Gebirge 1, Austria	*Ursus spelaeus*	32,000	2.20	2.81	0.41	3.465	Y
MH S	Vindija, Croatia	*Ursus spelaeus*	40–50,000	2.94	2.96	0.283	0.135	N
MH T	Vindija, Croatia	*Ursus spelaeus*	80–90,000	3.72	3.1	0.265	0.21	N
Me2-95	Mustang Cave	*Homo sapiens*	300	2.66	2.6	0.504	4.455	N
Me3-104	Mustang Cave	*Homo sapiens*	300	2.44	2.7	0.44	5.505	N
D	Greece (exact location unknown)	*Homo sapiens*	Unknown	3.73	3.07	0.377	1.02	Y
E	Greece (exact location unknown)	*Homo sapiens*	Unknown	3.86	2.97	0.362	0.67	Y
F	Greece (exact location unknown)	*Homo sapiens*	Unknown	5.11	3.46	0.215	0.145	Y
H	Greece (exact location unknown)	*Homo sapiens*	Unknown	5.73	4.03	0.176	0.415	N
J	Greece (exact location unknown)	*Homo sapiens*	Unknown	20.01	4.3	0.224	0.165	N
K	Greece (exact location unknown)	*Homo sapiens*	Unknown	4.31	3.91	0.321	0.525	N
L	Greece (exact location unknown)	*Homo sapiens*	Unknown	3.55	3.49	0.321	0.73	Y
O	Greece (exact location unknown)	*Homo sapiens*	Unknown	4.75	3.26	0.363	1.035	Y
P	Greece (exact location unknown)	*Homo sapiens*	Unknown	5.09	3.55	0.401	0.095	Y
R	Greece (exact location unknown)	*Homo sapiens*	Unknown	4.82	3.3	0.454	0.665	Y
T	Greece (exact location unknown)	*Homo sapiens*	Unknown	4.57	3.4	0.273	1.075	Y
U	Greece (exact location unknown)	*Homo sapiens*	Unknown	4.09	3.79	0.473	0.975	Y
V	Greece (exact location unknown)	*Homo sapiens*	Unknown	4.61	3.36	0.296	1.68	Y
W	Greece (exact location unknown)	*Homo sapiens*	Unknown	4.65	3.67	0.244	0.945	Y
X	Greece (exact location unknown)	*Homo sapiens*	Unknown	4.17	3.5	0.523	1.42	Y
SI3	Siegsdorf, Germany	*Panthera leo spelaea*	47180 + 1190/-1040	2.99	2.76	0.469	3.83	Y
KU3	Tischhofer Cave, Austria	*Panthera leo spelaea*	31,890±300	2.98	2.91	0.399	3.65	Y

measurement represents the average of a and b (for a needle-like crystal) or $2a$ (for a plate-like crystal). The shape parameter (η) of the crystallite is the mean square deviation of the obtained shape function (defined as the spherically averaged intensity plotted against distance in reciprocal space) from a standardized Lorentzian function [13].

Fourier-transform infrared spectroscopy (FTIR) and elemental analysis were conducted by the Chemical and Material Analysis Unit at the Central Scientific Facilities of the University of Newcastle upon Tyne. FTIR spectra were used to generate two indices of mineral alteration: splitting factor (SF), following the technique described in [40]; and carbonate:phosphate ratio (C:P),

using the method detailed in [41]. By this method, the carbonate and phosphate contents are not measured directly, but rather are determined by the ratio of the absorbance peaks in the spectrum. SF and C:P reflect the degree of order and composition within the crystallite lattice, respectively. The two are linked due to the structural change introduced into the crystal lattice via carbonate substitution; the loss of carbonate and corresponding decrease in strain during diagenesis drives an increase in crystallinity [34]. The whole bone nitrogen content was measured on a Carlo-Erba 1106 elemental analyser, providing a bulk measurement of weight percent nitrogen in the bone powder. Elemental analysis was run in duplicate for each sample, and the two values averaged.

3. Results

3.1. Comparison of SAXS measurements and other mineral diagenesis parameters

A complete set of results for each sample, including crystallite thickness, infrared splitting factor, and carbonate:phosphate ratio, is provided in Table 1. Table 2 illustrates the correlations observed between the different measurements taken, both for the entire sample set and for defined subsets. No significant correlation was observed between the diagenetic measurements made and either the age or species of the samples.

Figs. 1 and 2 show the relationship between crystallite thickness and infrared splitting factor and carbonate:phosphate ratio, respectively. The data points were split into two populations, based on the thickness measurements: crystals thicker than 5 nm (thick-crystal samples), and crystals thinner than 5 nm (thin-crystal samples). This separation was not made arbitrarily at the 5-nm mark; rather, this reflects a biological limitation on crystal growth past 5 nm thick in fresh, non-pathological bone. Both sets will contain samples that have undergone diagenetic alteration; the difference is in the extent and nature of the alteration. Two samples have been left out of the plots showing crystallite thickness altogether, as they had calculated thickness values greater than 20 nm.

This division into thin-crystal and thick-crystal samples was based on the observed correlations between crystallite thickness and the other measures of mineral alteration, as well as the presence of residual nitrogen. In thin-crystal samples, the positive correlation between thickness and splitting factor is significant; for thickness and carbonate:phosphate ratio, the correlation is negative and also significant. If the thick-crystal samples are included in the data set, these relationships become insignificant. Likewise, if the thick-crystal samples are treated as a separate set, there are still no significant correlations between thickness and other measures of mineral alteration. Thus, it is apparent that a link exists between crystal thickness measurements and FTIR measures of crystal order and composition, provided the change in crystal thickness is limited to within physiological parameters.

Fig. 3 illustrates the relationship between SF and C:P. These variables are weakly correlated in the thin- and

Table 2
Details of statistical correlations between all variables in sample sets identified (significant results are shown with level of significance)

Sample set	Measurements	Crystal thickness	Splitting factor	Carbonate:phosphate	Residual nitrogen
All samples	Crystal thickness	***	0.06	−0.01	0.08
	Splitting factor	0.06	***	−0.41 ($p < 0.01$)	−0.60 ($p < 0.01$)
	Carbonate:phosphate	−0.01	−0.41 ($p < 0.01$)	***	0.45 ($p < 0.01$)
	Residual nitrogen	0.08	−0.60 ($p < 0.01$)	0.45 ($p < 0.01$)	***
Thin-crystal samples	Crystal thickness	***	0.60 ($p < 0.01$)	−0.36 ($p < 0.01$)	−0.49 ($p < 0.01$)
	Splitting factor	0.60 ($p < 0.01$)	***	−0.37 ($p < 0.01$)	−0.64 ($p < 0.01$)
	Carbonate:phosphate	−0.36 ($p < 0.01$)	−0.37 ($p < 0.01$)	***	0.46 ($p < 0.01$)
	Residual nitrogen	−0.49 ($p < 0.01$)	−0.64 ($p < 0.01$)	0.46 ($p < 0.01$)	***
Thick-crystal samples	Crystal thickness	***	−0.04	0.12	0.33
	Splitting factor	−0.04	***	−0.53 ($p < 0.05$)	−0.52 ($p < 0.05$)
	Carbonate:phosphate	0.12	−0.53 ($p < 0.05$)	***	0.34
	Residual nitrogen	0.33	−0.52 ($p < 0.05$)	0.34	***
DNA-positive samples	Crystal thickness	***	0.85 ($p < 0.01$)	−0.58 ($p < 0.05$)	−0.89 ($p < 0.01$)
	Splitting factor	0.85 ($p < 0.01$)	***	−0.51	−0.82 ($p < 0.01$)
	Carbonate:phosphate	−0.58 ($p < 0.05$)	−0.51	***	0.53
	Residual nitrogen	−0.89 ($p < 0.01$)	−0.82 ($p < 0.01$)	0.53	***
DNA-negative samples	Crystal thickness	***	0.77 ($p < 0.01$)	−0.34	−0.24
	Splitting factor	0.77 ($p < 0.01$)	***	−0.61	−0.59
	Carbonate:phosphate	−0.34	−0.61	***	0.91 ($p < 0.01$)
	Residual nitrogen	−0.24	−0.59	0.91 ($p < 0.01$)	***

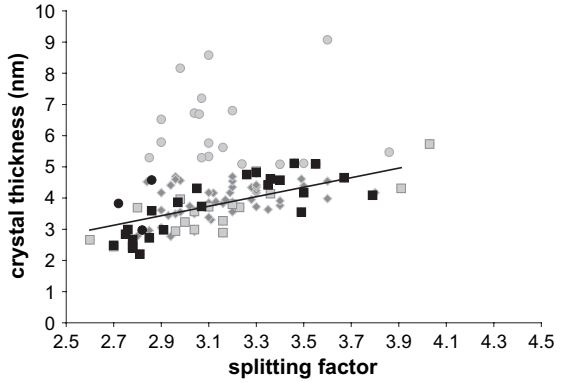

Fig. 1. Crystallite thickness shown plotted in relation to infrared splitting factor. Light circles are large thickness values (≥5 nm); dark diamonds are small thickness values. The squares represent the DNA sample set: dark squares are positive samples, and light squares are negative samples. Dark circles represent modern samples. The trend line illustrates the linear relationship between thickness and splitting factor for the thin-crystal sample subset ($p < 0.01$).

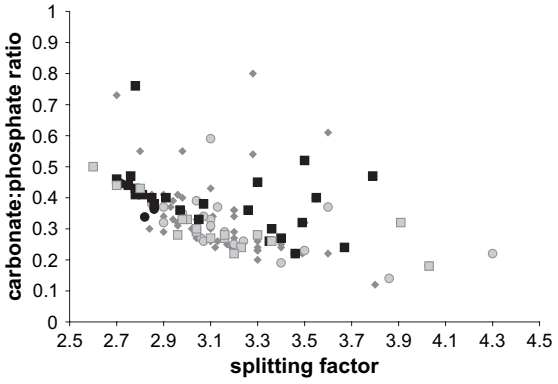

Fig. 3. Comparison of carbonate:phosphate ratio and splitting factor for all samples. Light circles are large thickness values (≥5 nm); dark diamonds are small thickness values. The squares represent the DNA sample set: dark squares are positive samples, and light squares are negative samples. Dark circles represent modern samples. The three samples showing considerable carbonate enrichment (C:P > 0.7) are all in the thin-crystal sample subset.

thick-crystal subsets, as well as the entire sample set, as was anticipated. The two measurements are related in that both reflect alteration to the crystal lattice; while C:P reflects crystal composition, particularly the inclusion of carbonate in the crystal structure, SF measures the crystallinity, in terms of strain and lattice perfection. Crystallite thickness appears to contribute little to this relationship in the sample set as a whole, as well as in the thick-crystal samples; the use of thickness as a controlling variable in partial correlation analysis made no difference to the result. In the thin-crystal samples, however, controlling for thickness reduced the correlation between SF and C:P to nearly zero. This could indicate that thickness is an intervening factor in the correlation between SF and C:P for crystallites limited to physiological parameters. Despite some high-C:P exceptions, these samples remain on a clear trajectory from physiological characteristics to low carbonate and reduced lattice strain, with limited change in crystal thickness.

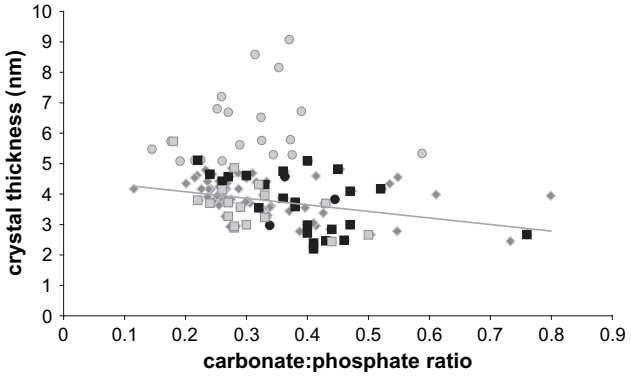

Fig. 2. Crystal thickness plotted against carbonate:phosphate ratio as determined from FTIR spectra. Light circles are large thickness values (≥5 nm); dark diamonds are small thickness values. The squares represent the DNA sample set: dark squares are positive samples, and light squares are negative samples. Dark circles represent modern samples. A weak negative relationship is seen between C:P ratio and small thickness samples only, as shown by the dark gray line ($p < 0.01$).

The crystal shape parameter (η) did not appear to correlate with any other mineral data parameter (data not shown); however, previous studies have shown that shape measurements can be dependent on the skeletal element examined [14] or on sample preparation methods such as crystallite dispersal [37], and is often the first mineral parameter to change during experimental diagenesis [20]. The range of crystal shapes found in these archaeological samples mostly lay within that seen in modern bone samples, and very little polydispersity was observed. Since different species and skeletal elements were used here, it is difficult to determine how much of this shape variation would be seen in a similar sample set of modern skeletons.

3.2. Measurements of mineral alteration and organic preservation

Fig. 4 shows the relationship between crystallite thickness and whole bone nitrogen. As before, the two anomalously thick samples have been left out of the plot. A weak negative correlation between thin-crystal samples and residual nitrogen can be seen: crystals grow thicker as the samples lose organic material. In the samples with crystallites larger than physiologically possible ($T > 5$ nm), the correlation is weaker and insignificant; this is also true if the thin-crystal and thick-crystal samples are considered to be one sample set.

Figs. 5 and 6 show the results of FTIR spectral measurements against whole bone nitrogen. A negative

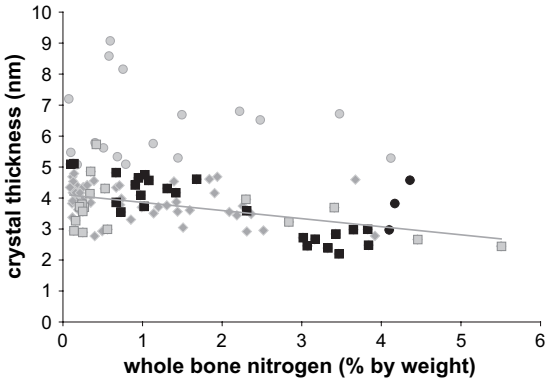

Fig. 4. Crystal thickness plotted against whole bone nitrogen by weight. The thick-crystal samples (light circles) show no clear relationship between thickness and nitrogen content. The thin-crystal samples (dark diamonds) show a weak linear relationship ($p < 0.01$) between thickness and nitrogen, illustrated by the gray line. Samples that were positive for amplifiable ancient DNA (dark squares) tend to cluster together. Light circles are large thickness values (≥ 5 nm); dark diamonds are small thickness values. The squares represent the DNA sample set: dark squares are positive samples, and light squares are negative samples. Dark circles represent modern samples.

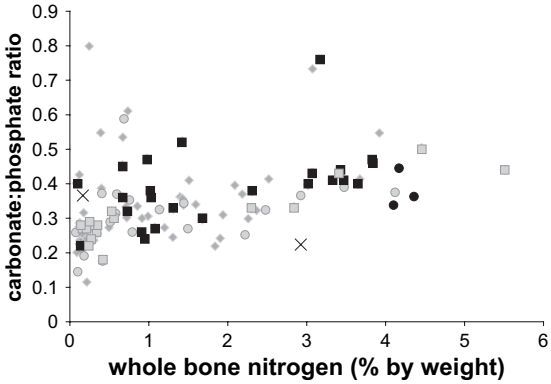

Fig. 6. Carbonate:phosphate ratio plotted against whole bone nitrogen by weight. Light circles are large thickness values (≥ 5 nm); dark diamonds are small thickness values. The squares represent the DNA sample set: dark squares are positive samples, and light squares are negative samples. Dark circles represent modern samples. The thin- and thick-crystal samples, while still distinguished by different markers, form a coherent data set. The majority of the DNA-positive samples form a discrete cluster at high nitrogen and moderate C:P. The two crosses represent the samples with abnormally thick crystallites ($T > 20$ nm).

correlation between SF and %N and a weak positive correlation between C:P and %N are observed for the sample set as a whole, including both thin- and thick-crystal samples. These correlations are slightly stronger in the thin-crystal sample set. In the thick-crystal samples, however, the correlation between %N and SF is slightly weaker, and the correlation between %N and C:P is weak and insignificant. Moreover, the thick-crystal population is invisible by any measurement other than SAXS: while these samples are highlighted on the plots shown, the thick-crystal population disappears into the bulk of the sample set. The two anomalously thick samples are presented on these plots, and do not stand out from the rest of the data set, despite having crystal thickness measurements of $T > 20$ nm.

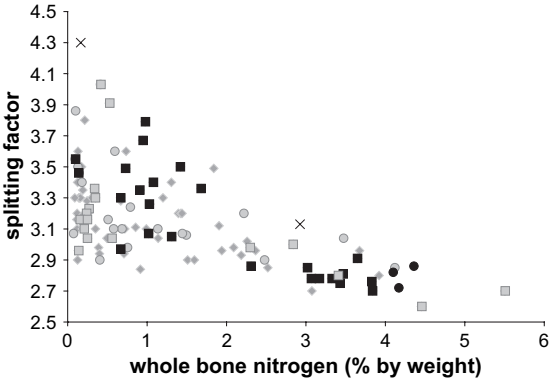

Fig. 5. Infrared splitting factor plotted against whole bone nitrogen by weight. A strong relationship ($p < 0.01$) between mineral and organic parameters is seen for the DNA-positive samples. Moreover, the thin- and thick-crystal samples merge into one population, and are not separated by any systematic difference in splitting factor. The relationship between SF and nitrogen for the DNA-negative samples is weak. Light circles are large thickness values (≥ 5 nm); dark diamonds are small thickness values. The squares represent the DNA sample set: dark squares are positive samples, and light squares are negative samples. Dark circles represent modern samples. The two crosses represent the samples with abnormally thick crystallites ($T > 20$ nm).

The preservation of ancient DNA in bone could also be considered here, since a subset of the archaeological samples had previously been used in ancient DNA analysis [2,11,26,36] (M. Hofreiter et al., unpublished data); both successes and failures are shown in the tables and figures. The negative correlation between thickness and nitrogen is much stronger in the subset of thin-crystal samples that had previously been used successfully for ancient DNA analysis; this is also true for SF and nitrogen, and SF and thickness. The ancient DNA failures, by contrast, did not cluster, but were instead fairly evenly distributed amongst the entire sample set; however, they were more represented by low nitrogen values. From this, it is evident that DNA-positive samples are unique in terms of the relationships between residual nitrogen content and two of the three measures of mineral alteration, namely infrared splitting factor and crystallite thickness. For a sample to be likely to contain DNA, it should also fall into this cluster, defined by high residual nitrogen, low SF, and small crystallite thickness measurement.

DNA-negative samples, in contrast, showed a significant strong correlation between nitrogen and carbonate content. The close relationship between C:P and %N in these samples probably reflects the slightly skewed distribution of the DNA-negative samples, which cluster at the extreme low end of nitrogen preservation;

furthermore, the DNA-negative samples are not represented amongst the small number of samples showing carbonate enrichment, whereas a few of the DNA-positive samples show some evidence of elevated carbonate. The DNA-negative samples used in this study showed very little variation in C:P, with most samples showing neither significant depletion nor enrichment. Since greater variation in C:P was seen in the much larger set of DNA-untested cases, it may be an accident of sampling that the range of variation in the negative samples was so low.

Again, the crystallite shape parameter, η, did not correlate well with nitrogen preservation. This result suggests that mineral crystallite shape change can occur without a significant disruption to the organic fraction of bone. It is possible that this is not always the case, however, as the shape parameter values for the samples used in this study in most cases fell within the range of variation of unaltered bone.

3.3. Multivariate statistical analysis

To clarify the relationships between mineral diagenesis and nitrogen preservation using the four parameters described here, principal components analysis was employed. It was hoped that this would elucidate underlying patterns in the data that were difficult to visualize with bivariate statistics alone. For each set of data measurements, only principal components with eigenvalues >1 were considered. In the sample set as a whole, the first two principal components accounted for 75% of the variance in the data (50% and 25%, respectively). In this case, SF and %N correlated closely with the first principal component, while thickness was strongly related to the second. This implies that the main predictors of DNA survival in the sample set used here are SF, %N, and crystal thickness taken together.

4. Discussion

4.1. SAXS and mineral diagenesis

Bone crystallite shape and thickness measurements were obtained from SAXS data in the course of this study. A third parameter, orientation, can be obtained from SAXS scattering patterns of bone sections [13]; however, for the powdered samples examined here, the native orientation of the mineral component had been disrupted by grinding, and the signal therefore tended toward isotropy. As stated previously, the shape parameter as determined in these experiments bore little or no relation to any other measurement observed. It is possible that for highly diagenetically altered bone crystallites, a change in shape may appear as polydispersity due to the limitations of resolution with the SAXS experimental setup used here; this may particularly affect the thick-crystal samples ($T > 5$ nm). Due to this limitation, and the observation that for these experiments no correlations between the shape parameter and indicators of preservation were observed, the subsequent discussion will focus on the contribution of bone crystallite thickness measurements.

The correlations observed between SAXS measurements of crystal thickness and both infrared splitting factor (SF) and carbonate:phosphate ratio (C:P) were anticipated. Both high SF and low C:P are thought to relate to increased crystallite perfection, larger size, and reduced strain due to the loss of carbonate in the hydroxyapatite lattice. This relationship was only true, however, for crystallites with thicknesses below 5 nm (thin-crystal samples). It is interesting to note that a wide range of SF values are possible for a given crystallite thickness, indicating a substantial degree of flexibility in crystal lattice order that can occur without actual change in crystal size.

SAXS thickness measurements revealed an additional population of samples with enlarged crystallites, above 5 nm (thick-crystal samples). For these thick-crystal samples, the correlations between thickness and crystal order and perfection were weak and insignificant; apparently, lattice perfection was not directly related to the often-substantial crystal growth observed in some samples. In non-pathological bone, crystallites are prevented from reaching thicknesses of 5 nm and above in vivo by the biological space limitation probably imposed by the collagen matrix; therefore, this increase in size reflects diagenetic alteration of the biogenic mineral. SF and C:P, as measurements of lattice perfection, can measure strain and composition in crystal lattices regardless of crystal size, and hence may not reflect the full extent of diagenetic alteration to bone mineral. SAXS, on the other hand, is providing a direct indication of the preservation or disruption of the biogenic crystal structure itself. The presence of this population of crystals that have lost their biogenic structure, yet retain their lattice characteristics indicates that crystal lattice perfection and retention of biogenic structure may be only weakly related in diagenesis (c.f. [27]).

It becomes apparent that there are multiple crystallite populations in this data set, which are revealed by crystallite thickness measurements. The first, the thin-crystal samples, are following a standard pathway of mineral diagenesis: as organic material is lost, the crystallites thicken and take on a more thermodynamically stable form, with decreased carbonate content and increased splitting factor. The second population consists of the thick-crystal samples that have little or no remaining organic material, and which have greatly decreased carbonate and increased splitting factor, indicating reduced strain and changed composition in the crystal lattice. Crystallites in these samples are able

to grow to sizes that are much thicker than biogenic values, due to the increased stability of the crystal lattice and the absence of a possibly inhibitory organic fraction. The third population, however, is unusual in that it contains thick-crystal samples with near-modern values of C:P and SF. Most of these samples have also lost the residual nitrogen that would indicate a remaining organic phase, but there are some of these cases that also contain greater than 1% N. Many of these are from the same site, Wierchowska Gorna in Poland; hence, this distinctive pattern may reflect a particular geological effect of preservation. This characteristic may reflect the subsequent infilling of the bone structure with authigenic cave mineral, which is similar in lattice characteristics to bone apatite. If the infilling occurred after the organic material had been lost, then the samples may appear to contain large carbonated apatite crystallites. If, however, the infilling occurred while some organic material remained in the bone sample, then the sample may appear to have not only large thick crystallites of carbonated apatite, but may also still contain substantial organic material, which was sheltered from further diagenetic loss.

Two samples in particular had crystallites with thickness almost 10 times that of fresh bone crystallites, and yet neither stood out from the rest of the samples in terms of SF or C:P. In our previous experience, crystals so enlarged have only been seen in experimentally cremated samples. For these samples, heating prior to burial or other similar post-mortem treatment seems unlikely, since they both are Pleistocene cave bear (*Ursus spelaeus*) remains, albeit from different sites. It is possible that these measurements of crystallites over 20 nm thick were caused by the limitation of the SAXS measurement itself. The range of crystallite thicknesses that can supposedly be measured by SAXS has been given as 0.5–50 nm [14]; however, at increasing thickness values, distortion from the crystal can affect the measurement of crystal characteristics. The crystal thicknesses of these samples could be measured more accurately with an increased sample to detector distance, effectively using an ultra-small angle X-ray scattering (USAXS) technique. Interestingly, one of these samples still contained over 2% nitrogen; mineral infilling prior to the loss of all organic residues may have protected the remaining protein from further alteration.

The remainder of the thick-crystal samples are more easily explained by the limitations of the sample set itself, rather than that of the apparatus or experimental procedure. All the archaeological bones used in this study have originated in cave sites, where apatite and carbonated apatite can often be precipitated diagenetically as stable mineral elements [23]. In such an environment, parameters that measure lattice perfection may not change even though the crystallites themselves undergo profound alteration. It is in these samples that the difference between a lattice measurement, such as SF or C:P, and a real dimensional measurement, such as SAXS thickness, becomes clear; alteration in apparently well-preserved, stable samples becomes evident when SAXS is used as a complementary technique.

4.2. SAXS and the prediction of organic preservation

The relationships between organic preservation—measured as weight percent nitrogen in whole bone powder (%N)—and the three mineral measurements were investigated. For all three mineral parameters, the samples were split into thin-crystal and thick-crystal subsets in the plots shown. For plots of SF or C:P versus %N, all samples were used, including the two extreme outliers with crystallite thickness greater than 20 nm. These samples were left out of the plot of thickness versus %N for ease of visualization, but were included for the purposes of statistical analysis.

All three mineral measurements had a relatively weak negative relationship to nitrogen content of the sample; of these, SF had the closest correlation to nitrogen level, and was also the only measurement to correlate significantly with nitrogen for the sample set as a whole. This, presumably, reflected the presence of outliers in the thickness measurements, which fell into the thick-crystal range. The correlations are stronger between all the mineral measurements and nitrogen content when only the thin-crystal sample set is considered, although SF still seems to be a better indicator of nitrogen levels at this stage. Without measurements of crystallite thickness, however, the alteration in some samples is not apparent.

Since SAXS is a direct measurement of biogenic structure, it will show diagenetic changes that may not be reflected in lattice perfection indices. If the mineral surface and intact structure do indeed play a role in biomolecular preservation, then SAXS may be not only a better indicator of the true extent of mineral alteration but also an 'early-warning' system to detect the beginning of diagenetic change. For all three mineral measurements, a wide range of variation in mineral characteristics was seen at the end of the scale where no organic matrix remained, indicating that once the regulation of the collagenous component was lost, the mineral was free to change, and crystal lattice, shape and thickness tended to adopt the most stable configuration available in the burial microenvironment.

A small subset of samples that were known positives for ancient DNA ($n = 26$) was included in the overall sample set, as well as a subset of samples that had failed to produce any viable ancient DNA sequences ($n = 17$). Both these subsets were plotted separately to show their relationship to the remainder of the population. The successes were primarily thin-crystal ($T < 5$ nm) samples, with only two samples just over 5 nm thick. This

reinforces the theory that DNA may be bound to the mineral surface: if crystals thicken substantially and the mineral surface is altered, the DNA may be severely damaged or lost. DNA-positive samples clustered together at values of high residual nitrogen, low SF, modern to high C:P, and modern thickness. There were one or two outliers in this sample set, but the majority of the DNA-positive samples fit into this narrow range of diagenetic characteristics. By contrast, the DNA-negative samples were evenly distributed amongst the entire sample set, with the only clustering evident at the low-nitrogen end of the preservational scale; however, only two were in the thick-crystal set. The majority of thick-crystal samples, unfortunately, remain untested for ancient DNA, but it is our prediction that DNA would not survive in these samples.

These results point to a specific diagenetic 'path' that samples must remain on, in order for amplifiable DNA to survive; the best samples have little or no mineral alteration and nearly modern levels of nitrogen remaining, but a certain amount of mineral change and nitrogen loss is tolerable as long as the two remain closely related. Eventually a stage is reached at which too much DNA has been lost or degraded to be amplifiable. Using the close relationships between SF, thickness, and residual nitrogen measurements, samples likely to contain ancient DNA could be identified using methods that are faster and simpler than the more laboratory-intensive methods of ancient DNA prediction, such as amino acid racemization.

5. Conclusions

We have successfully employed a new bulk screening technique, SAXS, for examining mineral alteration in archaeological bone. Further work is required to fully elucidate the link between alteration in crystallite thickness, and possibly crystal habit, and the preservation of organic material in bone. We have shown preliminary evidence of such a link. In future, a similar study using bones from non-cave sites, where mineral diagenesis follows more diverse pathways, will establish more clearly the use of SAXS measurements to determine preservation and retrievability of organic material.

The link found here between crystal thickness and other measures of mineral alteration has also reinforced conclusions reached in our earlier work involving a microfocus SAXS technique. Previously, we had postulated that alteration to mineral surfaces observed using SAXS was linked to loss of organic material and changes to SF measurements [39]. While we were able to determine crystal shape and size using SAXS over small areas within a bone cross-section, we lacked a similar microanalysis technique to examine the corresponding infrared spectrum or organic residue present at these interior sites. The development of a bulk technique for examining crystal shape and thickness in conjunction with well-established infrared spectroscopy and elemental analysis techniques has lent added confidence to our earlier work on intra-bone variability of preservation.

Acknowledgements

We are grateful to J. Weir (University of Stirling) for his assistance with data collection on the NanoSTAR, and to D. Dunbar (University of Newcastle upon Tyne) for assistance with FTIR data collection. Part of this work was carried out while J.C.H. was funded by a Wellcome Trust PhD studentship in Bioarchaeology. We thank D. Bonjean and M. Otte (Scladina Cave, Belgium), C. Hanni (CNRS, University of Lyon 2), I. Barnes (University College London), J. Burger (Johannes-Gutenberg-Universitat Mainz), M. Hofreiter (Max-Planck Institute for Evolutionary Anthropology, Leipzig), M. Evison (University of Sheffield), T. Torres (Biomolecular Stratigraphy Laboratory, Madrid School of Mines) and the curators of the Tyne and Wear Museums, Newcastle upon Tyne, for graciously providing archaeological and modern samples for analysis. We acknowledge the support of SHEFC and Biodermis, Ltd., under the auspices of the Joint Research Equipment Initiative, for the purchase of the NanoSTAR apparatus. We are also grateful to two anonymous reviewers for their helpful comments.

References

[1] H. Bocherens, D. Drucker, Trophic level isotopic enrichment of carbon and nitrogen in bone collagen: case studies from recent and ancient terrestrial ecosystems, International Journal of Osteoarchaeology 13 (1–2) (2003) 46–53.

[2] J. Burger, W. Rosendahl, O. Loreille, H. Hemmer, T. Eriksson, A. Götherström, J. Hiller, M.J. Collins, T. Wess, K.W. Alt, Molecular phylogeny of the extinct cave lion *Panthera leo spelaea*, Molecular Phylogenetics and Evolution 30 (3) (2004) 841–849.

[3] N.P. Camacho, S. Rinnerthaler, E.P. Paschalis, R. Mendelsohn, A.L. Boskey, P. Fratzl, Complementary information on bone ultrastructure from scanning small-angle X-ray scattering and Fourier-transform infrared microspectroscopy, Bone 25 (3) (1999) 287–293.

[4] A.M. Child, Towards an understanding of the microbial decomposition of archaeological bone in the burial environment, Journal of Archaeological Science 22 (1995) 165–174.

[5] M.J. Collins, A.M. Child, A.C.T. van Duin, C. Vermeer, Is osteocalcin stabilised in ancient bones by adsorption to bioapatite?, Ancient Biomolecules 2 (1998) 223–233.

[6] M.J. Collins, A.M. Gernaey, C.M. Nielsen-Marsh, C. Vermeer, P. Westbroek, Slow rates of degradation of osteocalcin: green light for fossil bone protein? Geology 28 (12) (2000) 1139–1142.

[7] M.J. Collins, C.M. Nielsen-Marsh, J. Hiller, C.I. Smith, J.P. Roberts, R.V. Prigodich, T.J. Wess, J. Csapò, A.R. Millard, G. Turner-Walker, The survival of organic matter in bone: a review, Archaeometry 44 (3) (2002) 383–394.

[8] M.J. Collins, M.S. Riley, A.M. Child, G. Turner-Walker, A basic mathematical simulation of the chemical degradation of ancient collagen, Journal of Archaeological Science 22 (1995) 175–183.
[9] A. Cooper, H.N. Poinar, Ancient DNA: do it right or not at all, Science 289 (2000) 1139.
[10] A. Cooper, R. Wayne, New uses for old DNA, Current Opinion in Biotechnology 9 (1998) 49–53.
[11] M.P. Evison, N.R.J. Fieller, D.M. Smillie, Ancient HLA: a preliminary survey, Ancient Biomolecules 3 (1) (1999) 1–28.
[12] M.J. Farquharson, R.D. Speller, M. Brickley, Measuring bone mineral density in archaeological bone using energy-dispersive low angle X-ray scattering techniques, Journal of Archaeological Science 24 (1997) 765–772.
[13] P. Fratzl, M. Groschner, G. Vogl, H. Plenk, J. Eschberger, N. Fratzl-Zelman, K. Koller, K. Klaushofer, Mineral crystals in calcified tissues: a comparative study by SAXS, Journal of Bone and Mineral Research 7 (3) (1992) 329–334.
[14] P. Fratzl, S. Schreiber, K. Klaushofer, Bone mineralization as studied by small-angle X-ray scattering, Connective Tissue Research 34 (4) (1996) 247–254.
[15] P. Fratzl, S. Schreiber, A. Boyde, Characterization of bone mineral crystals in horse radius by small-angle X-ray scattering, Calcified Tissue International 58 (1996) 341–346.
[16] A. Götherström, M.J. Collins, A. Angerbjörn, K. Lidén, Bone preservation and DNA amplification, Archaeometry 44 (3) (2002) 395–404.
[17] P.V. Hauschka, F.H. Wians Jr., Osteocalcin–hydroxyapatite interaction in the extracellular organic matrix of bone, The Anatomical Record 224 (2) (1989) 180–188.
[18] R.E.M. Hedges, Bone diagenesis: an overview of processes, Archaeometry 44 (3) (2002) 319–328.
[19] R.E.M. Hedges, A.R. Millard, A.W.G. Pike, Measurements and relationships of diagenetic alteration of bone from three archaeological sites, Journal of Archaeological Science 22 (1995) 201–209.
[20] J.C. Hiller, T.J.U. Thompson, M.P. Evison, A.T. Chamberlain, T.J. Wess, Bone mineral change during experimental heating: an X-ray scattering investigation, Biomaterials 24 (28) (2003) 5091–5097.
[21] M. Jackes, R. Sherburne, D. Lubell, C. Barker, M. Wayman, Destruction of microstructure in archaeological bone: a case study from Portugal, International Journal of Osteoarchaeology 11 (6) (2001) 415–432.
[22] K. Johnsson, Chemical dating of bones based on diagenetic changes in bone apatite, Journal of Archaeological Science 24 (1997) 431–437.
[23] P. Karkanas, O. Bar-Yosef, P. Goldberg, S. Weiner, Diagenesis in prehistoric caves: the use of minerals that form in situ to assess the completeness of the archaeological record, Journal of Archaeological Science 27 (2000) 915–929.
[24] G.J. van Klinken, Bone collagen quality indicators for palaeodietary and radiocarbon measurements, Journal of Archaeological Science 26 (1999) 687–695.
[25] J.N. Lanting, A.L. Brindley, Dating cremated bone: the dawn of a new era, Journal of Irish Archaeology IX (1998) 1–8.
[26] O. Loreille, L. Orlando, M. Patou-Mathis, M. Philippe, P. Taberlet, C. Hänni, Ancient DNA analysis reveals divergence of the cave bear, *Ursus spelaeus*, and brown bear, *Ursus arctos*, lineages, Current Biology 11 (2001) 200–203.
[27] L.M. Miller, V. Vairavamurthy, M.R. Chance, R. Mendelsohn, E.P. Paschalis, F. Betts, A.L. Boskey, In situ analysis of mineral content and crystallinity in bone using infrared micro-spectroscopy of the ν_4 PO_4^{3-} vibration, Biochimica et Biophysica Acta 1527 (2001) 11–19.
[28] C.M. Nielsen-Marsh, P.H. Ostrom, H. Gandhi, B. Shapiro, A. Cooper, P.V. Hauschka, M.J. Collins, Sequence preservation of osteocalcin protein and mitochondrial DNA in bison bones older than 55 ka, Geology 30 (12) (2002) 1099–1102.
[29] A. Person, H. Bocherens, J.-F. Saliege, F. Paris, V. Zeitoun, M. Gerard, Early diagenetic evolution of bone phosphate: an X-ray diffractometry analysis, Journal of Archaeological Science 22 (1995) 211–221.
[30] F. Petchey, T. Higham, Bone diagenesis and radiocarbon dating of fish bones at the Shag River Mouth site, New Zealand, Journal of Archaeological Science 27 (2000) 135–150.
[31] I. Reiche, L. Favre-Quattropani, T. Calligaro, J. Salomon, H. Bocherens, L. Charlet, M. Menu, Trace element composition of archaeological bones and post-mortem alteration in the burial environment, Nuclear Instruments and Methods in Physics Research B 150 (1999) 656–662.
[32] A. Sillen, A. Morris, Diagenesis of bone from Border Cave: implications for the age of the Border Cave hominids, Journal of Human Evolution 31 (1996) 499–506.
[33] A. Sillen, J. Parkington, Diagenesis of bones from Eland's Bay Cave, Journal of Archaeological Science 23 (1996) 535–542.
[34] T.A. Surovell, M.C. Stiner, Standardizing infrared measures of bone mineral crystallinity: an experimental approach, Journal of Archaeological Science 28 (2001) 633–642.
[35] J.D. Termine, A.S. Posner, Infrared determination of the percentage of crystallinity in apatitic calcium phosphates, Nature 211 (1966) 268–270.
[36] C.S. Troy, D.E. MacHugh, J.F. Bailey, D.A. Magee, R.T. Loftus, P. Cunningham, A.T. Chamberlain, B.C. Sykes, D.G. Bradley, Genetic evidence for Near Eastern origins of European cattle, Nature 410 (2001) 1088–1091.
[37] E. Wachtel, S. Weiner, Small-angle X-ray scattering study of dispersed crystals from bone and tendon, Journal of Bone and Mineral Research 9 (10) (1994) 1651–1655.
[38] T.J. Wess, M. Drakopoulos, A. Snigirev, J. Wouters, O. Paris, P. Fratzl, M. Collins, J. Hiller, K. Nielsen, The use of small-angle X-ray diffraction studies for the analysis of structural features in archaeological samples, Archaeometry 43 (1) (2001) 117–129.
[39] T. Wess, I. Alberts, J. Hiller, M. Drakopoulos, A.T. Chamberlain, M. Collins, Microfocus small-angle X-ray scattering reveals structural features in archaeological bone samples: detection of changes in bone mineral habit and size, Calcified Tissue International 70 (2) (2002) 103–110.
[40] S. Weiner, O. Bar-Yosef, States of preservation of bones from prehistoric sites in the Near East: a survey, Journal of Archaeological Science 17 (2) (1990) 187–196.
[41] L.E. Wright, H.P. Schwarcz, Infrared and isotopic evidence for diagenesis of bone apatite at Dos Pilas, Guatemala: palaeodietary implications, Journal of Archaeological Science 23 (6) (1996) 933–944.